Diamond & Related Materials 136 (2023) 109926

Contents lists available at ScienceDirect

Diamond & Related Materials

journal homepage: www.elsevier.com/locate/diamond

Adhesion effects on free-standing indentations for graphene oxide

E. Alejandra Huitrón Segovia [a,b], D. Torres-Torres [a,*], A. Garcia-Garcia [b,*]

[a] Laboratorio de Análisis de Integridad en Desempeño Mecánico de Dispositivos y Materiales Avanzados, CIMAV, Apodaca N.L., Mexico
[b] Grupo de Síntesis y Modificación de Nanoestructuras y Materiales 2D, CIMAV, Apodaca N.L., Mexico

ARTICLE INFO

Keywords:
Graphene oxide
Free-standing indentation
Nanoindentation

ABSTRACT

Three-layer graphene oxide sheets rich in epoxy and hydroxyl groups were obtained by oxidation and chemical exfoliation and analyzed by free-standing indentations. This work compares the wrinkled surface behavior before and after loading and the relation with the adhesion effect. During free-standing indentation, mechano-chemical effects are presented between the tip and graphene oxide, a widely known problem that prevents obtaining accurate measurements. It is well known that adhesion is ruled by wrinkles formed by oxygen functional groups. However, this work highlights that the mechano-chemical effect decreases substantially when increasing the tip radius. The morphological and chemical characteristics of the sample were determined by scanning electron microscopy and X-ray photoelectron spectroscopy techniques.

1. Introduction

Graphene oxide (GO) is a two-dimensional (2D) material with few layers and oxygen functional groups such as epoxide, carbonyl, carboxyl, and hydroxyl [1], that generate surface wrinkles and folds [2]. The wrinkles' dimensions and their fluctuation will influence their mechanical properties during the nanoindentation test [3].

Several works have reported that free-standing (FS) 2D materials had a small portion adhered to the substrate sidewall [4]. This adhesion (2–10 nm contact wide) is attributed to the Van der Waals (vdW) interaction between the FS 2D material and the substrate sidewall [5].

On this subject, adhesion at the substrate sidewall is affected by temperature, producing roughness fluctuations related to wrinkles in 2D materials [2,6].According to previous studies, the molecular dynamic simulation has shown that the adhered portion is fully delaminated when the FS membrane is stretched [7].

In addition, it has been reported that the major effect in the adhesion response can be related to the extrinsic wrinkles with nanometer magnitudes of height, mainly from its stored total potential energy [8].

Such extrinsic wrinkles, created by the solvent evaporation process once the sheets are deposited on a substrate, are related to the surface tension, which reduces the free energy at the sample surface, making it more stable thermodynamically [9].

Besides, these wrinkles can be produced due to the interaction between the tip and the sample during the indentation test [5]. Such work showed by MD simulations that although the AFM tip is typically assumed to be spherical and idealized as a point-load in the existing FS indentation models, a spherical tip can induce a very high-stress concentration and can even induce wrinkles fluctuations.

Thus, it could be argued that such high-stress concentration should also be responsible for the adhesion phenomenon between the indenter and GO sheets. Particularly, the physical mechanism of the indentation size effect proposed by the present work refers to an increased coefficient of friction, COF, during the indentation test when using a small R_{tip}, AFM cantilever, promoting their greater adhesion.

On the other hand, Begley [10] proposed the dependence on membrane radius relative to the tip radius for values of $a/R_{tip} < 30$, as expressed in the next equation:

$$\frac{h}{R_{tip}} = \frac{1}{q}\left(\frac{a}{R_{tip}}\right)^{\frac{2}{3}}\left(\frac{F}{R_{tip}E^{2D}}\right)^{\frac{1}{3}} \quad (1)$$

where h is penetration depth (displacement), a is membrane radius, R is tip radius, and F is load. Hence, rewritten Eq. (1), solving F and applying a/a at the left side, it is obtained the following expression:

$$\left(\frac{h}{a}\right)^3 (q^3 a)\, E^{2D} = F \quad (2)$$

which is the same cubic term as the equation reported by Ruiz-Vargas2011 and Cao2019 [11].

However, the 2D pre-stress, σ^{2D}, plays an important role, since the

* Corresponding authors.
E-mail addresses: david.torres@cimav.edu.mx (D. Torres-Torres), alejandra.garcia@cimav.edu.mx (A. Garcia-Garcia).

https://doi.org/10.1016/j.diamond.2023.109926
Received 17 October 2022; Received in revised form 22 March 2023; Accepted 10 April 2023
Available online 13 April 2023

contribution from stretching increases rapidly with increasing indentation displacement, becoming dominant when $h >> t$. [11].

For all the above reasons, we have decided to use the *F-h* relationship with dependence on membrane radius, tip radius, and the 2D pre-stress term, as discussed in the Materials and methods Section 2.

The present work aimed to demonstrate that the GO sheet mechanical performance is also highly influenced by the contact interaction between the tip and sample surface, which affects the adhesion phenomenon according to the revealed indentation size effect.

Particularly, the relationship between the indentation energy and the kinetic friction force, *P*, can be written in terms of the adhesion component (energy dissipated), *D*, and the applied load, *F*, and shown to be valid for several systems [12]:

$$P = C_1 D + C_2 F \tag{3}$$

The coefficient C_1 depends on the adhesion between the tip and sample surfaces, meanwhile, C_2 depends on the surface topography. However, according to Amontone' law, since the GO sheet is very smooth, the coefficient C_2 is too small, and hence, the dominating contribution to the kinetic friction force should come from the $C_1 D$ term.

2. Materials and methods

GO sheets were synthesized by a modified Hummer's method previously reported [13], which consisted of the graphite powder oxidation with a 3:1 mixture of H_2SO_4/HNO_3 and exfoliation with an excess of $KMnO_4$.

The structural and morphological characterizations of individual GO sheets were carried out using a field emission scanning electron microscopy system (FE-SEM) model Nova 200 (FEI Company) with a STEM detector. Meanwhile, the sample topography was evaluated with an Asylum MFP 3DSA AFM microscope in the standard AC-mode. The oxygen functionalities content was determined by X-ray spectroscopy (XPS) analysis performed with a Thermo Scientific Escalab 250Xi spectrometer using a monochromatic Al Kalpha source (1486.68 eV).

For the case of the nanoindentation test, when $h >> t$ condition is present, where *t* is the thickness of the sample, the relationship between *F* and *h*, of a clamped circular membrane pre-stressed subject to a point force at the center of the plate can be related to a/R_{tip} as follows:

$$F = \frac{2\pi a \sigma^{2D}}{ln\frac{a}{R_{tip}}}\left(\frac{h}{a}\right) + E^{2D}(q^3 a)\left(\frac{h}{a}\right)^3 \tag{4}$$

This relationship is validated for the condition of $a/R_{tip} < 30$, according to Ruiz-Vargas [14] and Cao [11], where $E^{2D} = E \cdot t$, with *E* as the bulk elastic modulus, and $\sigma^{2D} = \sigma \cdot t$, with σ as the bulk pre-stress.

Afterward, *q* is a dimensionless constant in the function of Poisson's ratio, ν, which was obtained by the following equation:

$$q = \frac{1}{(1.05 - 0.15\nu - 0.16\nu^2)} \tag{5}$$

Finally, according to the O/C ratio, in this work a negative Poisson's ratio for GO sheets through Eq. 6 was estimated, similar to the reported in the literature [15]:

$$\nu = (-0.84 * O/C) + 0.23 \tag{6}$$

The SPM images of suspended GO sheets before and after the cantilever and Berkovich nanoindentation were obtained by an Asylum MFP 3D-SA AFM microscope and by a TI-950 Triboindenter system, Hysitron Inc., respectively.

3. Results and discussion

Fig. 1a and b show the scanning electron microscopy (SEM) images

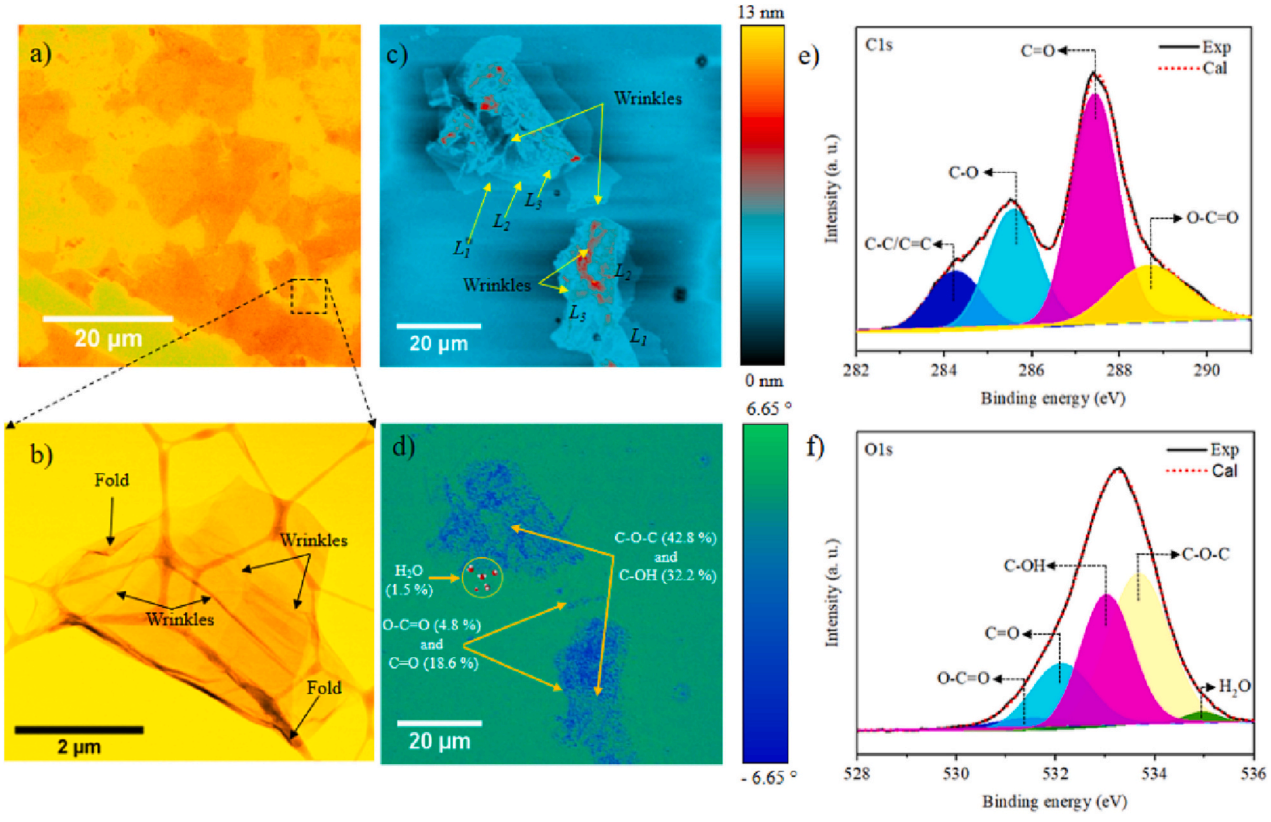

Fig. 1. SEM image of a) several and b) individual GO sheets. AFM image of three-layer GO sheet c) topography and d) phase image. XPS spectra for the e) C1s and f) O1s.

of several GO sheets with micrometric lateral sizes, folds, and wrinkles. In literature, oxygen group presence [9] is reported as one reason for these formations by sp^2 hybridization breaking. Fig. 1c shows three-layer GO sheets with a rough surface consisting of a lower layer (*L1*), a middle layer (*L2*), and an upper layer (*L3*). On the *L3* surface, the wrinkles are well-defined and more attributed to epoxy groups [16]. In addition, in Fig. 1c epoxy groups are represented with warm colors, while other oxygen groups are observed near the edges of each layer in cool colors. Meanwhile, in the phase response (Fig. 1d), the blue color was assigned to the hydroxyl and epoxy groups. In our work, phase response contrast is associated with greater adhesion between the tip-sample contact surfaces [17]. The higher interaction occurs as a result of the high surface energy (SE) of wrinkles, which is related to the co-valent bonding of the hydroxyl and epoxy groups [18]. The influence of the epoxy groups was studied by the Neumann method, showing SE values around 46.7 mJ/m^2, 54.8 mJ/m^2, and 62.1 mJ/m^2 for graphite, graphene, and GO [18,19]. Since adhesion is highly dependent on SE [20], XPS measurements were used to corroborate the present groups in our graphene oxide. First, the high-resolution XPS spectrum analysis for the C1s is shown in Fig. 1e. Peak deconvolution confirms the presence of different clusters located at 284.5 eV (C-C/C=C), 285.6 eV (C—O), 287.4 eV (C=O), and 288.7 eV (O-C=O). According to the literature, the peak located around 285.8 eV describes the interaction of carbon atoms with oxygen forming hydroxyl and epoxy functional groups whereas 288.7 eV describes the carbonyl groups related to carbon functionalized in COOH [21]. For O1s spectra, the deconvolutions are presented in Fig. 1f. The peaks located at 531.5 eV, 532.1 eV, 533 eV, 533.7 eV, and 534.9 eV were assigned to O-C=O (4.8 %), C=O (18.6 %), C-OH (32.2 %), C-O-C (42.8 %), and H_2O (1.5 %) respectively, confirming epoxy and hydroxyl groups in greater quantity. As described by the Lerf model [22], carboxyl and carbonyl groups are found mainly at the edges, and hydroxyl and epoxy are found in the basal planes of the GO sheets [23]. Finally, the C/O atomic ratio was calculated to be approximately 1.8, showing a high oxidation degree, that according to Jinfeng et al. [24], produces a significant effect on the SE. Studies indicate that a GO with a C/O ratio of 2.6 presents a value of 57.1 mJ/m^2 of the SE polar component, promoting stronger polar interactions [24]. Therefore, we expected a higher value of the SE polar component in our samples.

After chemical characterization, GO sheets were deposited by drop-casting in a grid with holes having 1 μm of diameter, see Fig. 2a. In this AFM image, it can be observed that the GO sheet is clamped to the substrate boundary and is indicated by the arrow. At the same time, the darker scale represents the free-suspended membrane. The blue line and the black dash line mark the profile sections that cross over the FS membrane before applying load. In addition, Fig. 2b shows the corresponding surface profiles, with the GO sheet section adhered to the substrate sidewall, while the FS membrane has a concave form. Reports indicate that the adhesion to the substrate boundary is enough to generate a pre-stress in a 2D material [6], where such interaction determines the orientation of the wrinkles according to the curvature of the sidewall [3]. Afterward, Fig. 2c shows the AFM image for the same FS membrane of the GO sheet after an indention load of 225 nN with the cantilever tip, which load-penetration curve was previously reported [13]. The blue line and the black dash lines are the two profiles that cross over the center of the FS membrane after applying load. In the same way, Fig. 2d shows the profiles of the indented GO sheet. The pulled-up effect suggests an adhesion between a tip and oxygen groups at the GO sheet surface, which probably was promoted by the electrostatic force resulting from the contact surface friction during the nano-indentation test [25]. Typically, the concentrated applied load with AFM nanoindentations on the 2D materials produces wrinkles with large amplitude [26], and similarly, in the present work, the same

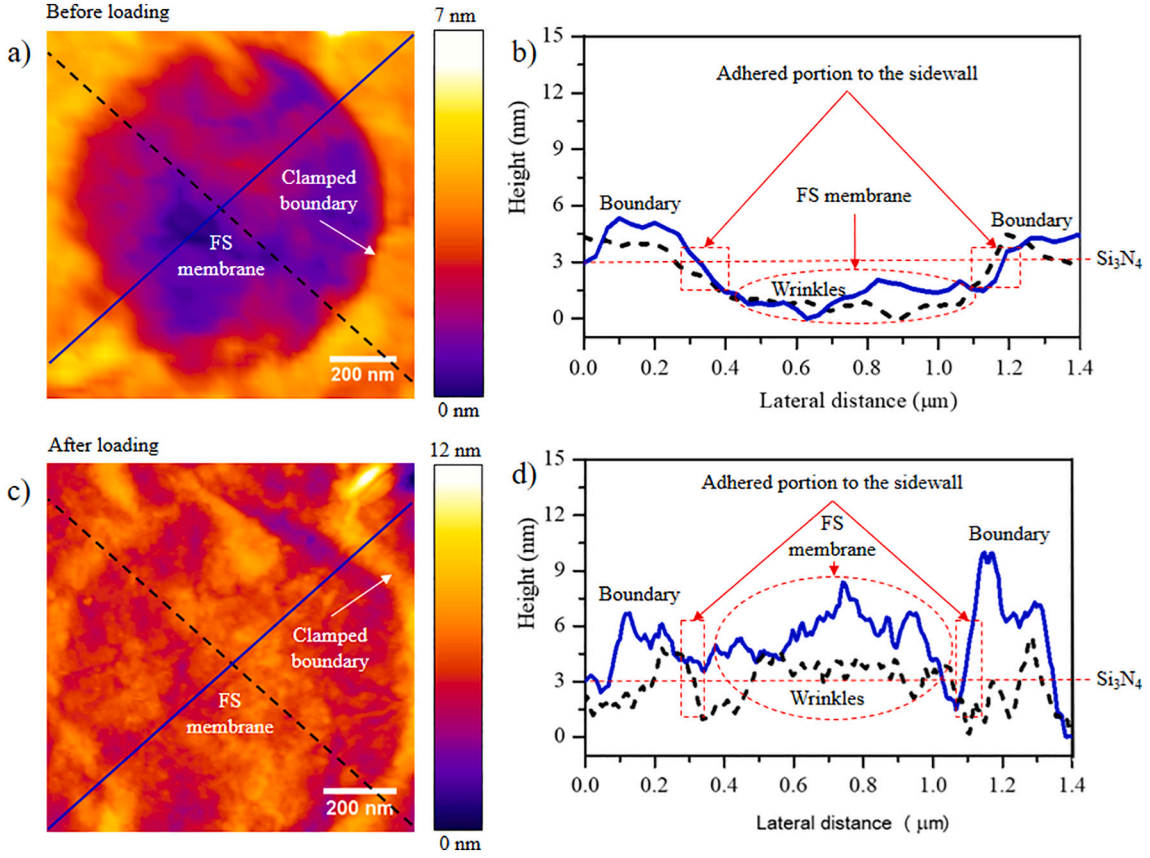

Fig. 2. GO sheet as deposited in FS membrane form: a) Morphological AFM image and b) surface profiles. GO sheet after indented by a cantilever tip: c) Morphological AFM image and d) surface profiles.

phenomenon was obtained, in which a major effect is indicated at the center of the penetrated FS membrane.

Analogously, Fig. 3a shows a scanning probe micrography (SPM) image of a GO sheet deposited in FS membrane form before indenting. The blue and black dash lines are profile sections that cross over the FS membrane before applying load. In addition, Fig. 3b shows the respective surface profiles, also having a GO sheet section adhered to the substrate sidewall, but the wrinkled FS membrane has a concave form. Successively, Fig. 3c shows an SPM image for the case of FS membrane after a nanoindentation load of 700 nN with the Berkovich tip, which load-penetration curve was also previously reported [13]. The blue line and the black dash lines are the two profile sections that cross over the center of the FS membrane after applying load. Furthermore, Fig. 3d shows the surface profiles, where the FS membrane's depth is more pronounced compared to the sample before the AFM nanoindentation. Such an effect occurs because of the sliding [27] between layers at the clamped boundary as indicated by arrows. However, one important characteristic is the wrinkles flattening, which suggests a major impact on the mechanical performance since more of them were involved in GO sheet deformation as well as in the tip/GO sheet contact area. Also, because the hydroxyl and epoxy groups should be removed through nanoindentation [28], the GO sheet will become almost free of wrinkles and an imminent SE reduction decreased the adhesion with the tip surface. According to this, the wrinkles flattening phenomenon avoids that the FS membrane had a recovering response, similar to a spring behavior, and remained in a concave form.

Once more, the mechanical properties of GO sheets were evaluated, additionally to the experimental measurements previously reported [13], but this time to find a possible relation with the adhesion mechanism described above. In this regard, Eq. (4) reported by Ruiz-Vargas and Cao was used [11,14], as discussed in the Materials and methods section.

Hence, for the AFM cantilever nanoindentation, a value of 2.2 N/m $\pm$ 0.01 N/m (2.5 GPa $\pm$ 12.9 MPa) for σ^{2D} was obtained, and E^{2D} resulted in 65 N/m $\pm$ 9 $\times$ 10^{-6} N/m (73.9 GPa $\pm$ 0.01 MPa), considering $\nu = -0.3$ for an O/C atomic ratio of 0.6. Afterward, the mechanical performance of a GO sheet was evaluated by the Berkovich nanoindentation, considering the same $\nu = -0.3$. As a result, an E^{2D} of 291 N/m $\pm$ 18.9 N/m (330.7 GPa $\pm$ 21.5 GPa) and a σ^{2D} of 5.4 N/m $\pm$ 0.04 N/m (6.1 GPa $\pm$ 47.6 MPa) were obtained.

The difference between AFM cantilever and Berkovich nanoindentations for σ^{2D} was an increase of about 59 %, while for E^{2D} such difference was also an increase of about 22 %.

The most apparent condition that affected the mechanical performance of the GO sheets during the nanoindentation tests should be the indenter size since the other conditions remained equal [13]. However, if a reduction in the oxidation degree is considered during the Berkovich test due to the wrinkles flattening and subsequent elimination of epoxy and hydroxyl groups, then, the reason for the adhesion effects should be related to the localized and lower wrinkles fluctuation during the AFM nanoindentation, which promotes the greater adhesion between the tip and the sample surface, see Fig. 2d. Given that, the GO sheet seems to have a strong adhesion with the AFM cantilever, probably due to electrostatic or Van der Waals forces between the tip and oxygen groups in the sample promoting higher COF values. In the present study, the Van der Waals forces can be neglected within the range of the distances involved [29].

Therefore, to verify such an assumption, the analysis of the coefficient of friction, during the nanoindentations of the GO sheets by AFM cantilever and Berkovich indenters, was carried out by FE simulations.

Considering the same conditions as reported in the literature [13], in the present work the simulation of Normal forces, *FN*, and Tangent forces, *FT*, against penetration depth, were acquired and are shown in Fig. 4a and b, respectively. In addition, COF=*FT/FN* are shown in Fig. 4c.

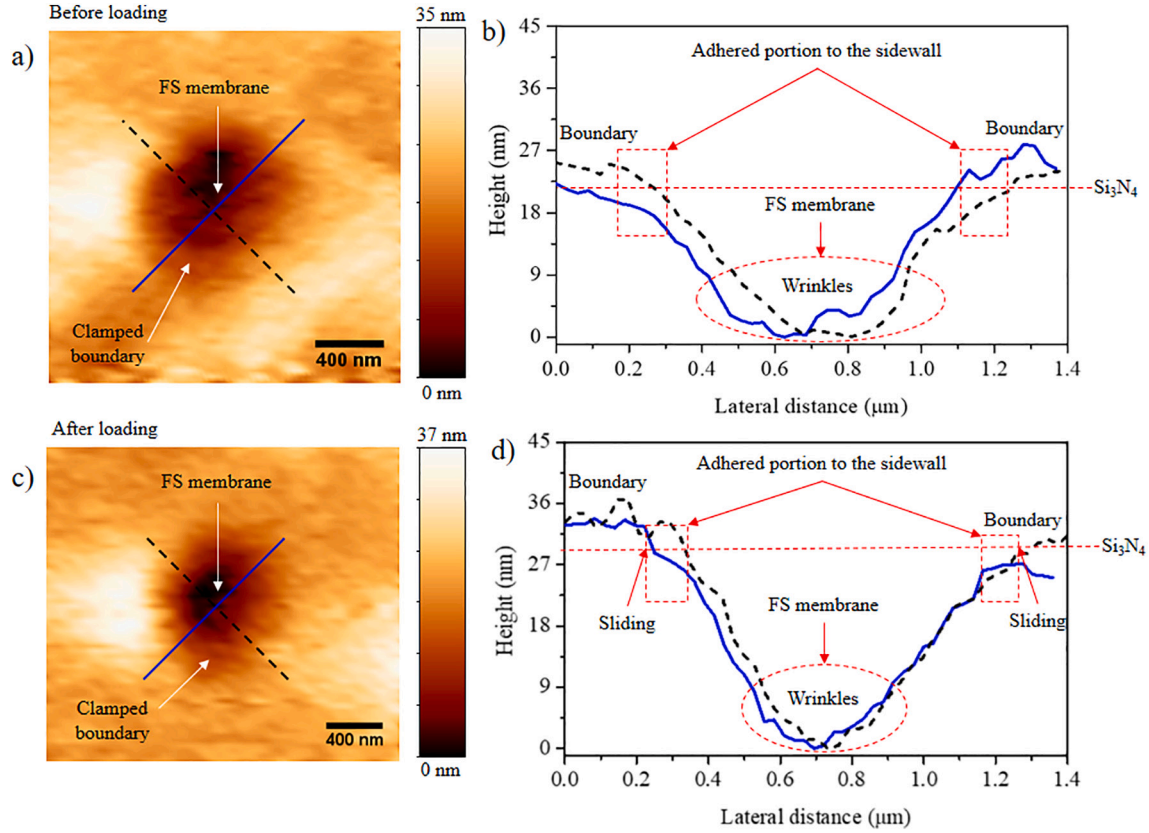

Fig. 3. GO sheet a) SPM image and b) surface profiles. GO sheet after indented by a Berkovich tip c) SPM image and d) surface profiles.

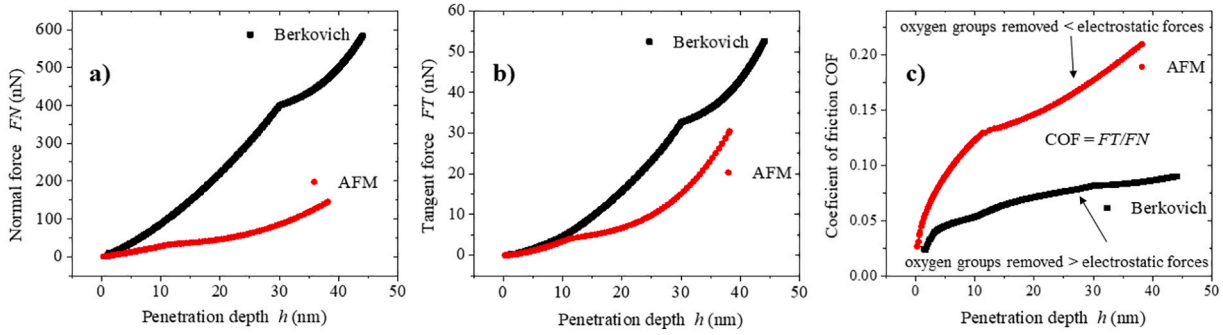

Fig. 4. FE results of AFM cantilever and Berkovich nanoindentation simulations: a) Normal forces, b) Tangent forces, and c) Coefficient of friction, against penetration depth.

Over the penetration depth of about 10 nm, the slope of all curves being somewhat steeper, but the *FT* slope of the AFM nanoindentation increases faster than that of the *FN*, but increasing in a gentler form for the Berkovich nanoindentation. This observation suggests that the increase in the tangent force with load, *F*, comes principally from the first term in Eq. (3), where the coefficient C_1 depends on the mutual adhesion of the tip and sample surfaces, which is nonlinear in *F*, and hence, not from the second term.

Also, comparing the similar penetration depths of both FE simulations, despite the Berkovich nanoindentation achieves *FN* and *FT* greater than the AFM cantilever nanoindentation, the AFM test reached COF values of approximately four times greater than those obtained in the Berkovich test.

Consequently, the adhesion effects seem to be a phenomenon induced by the tip/sample surface contact with a significant magnitude of COF, and therefore, probably related to higher electrostatic forces created. Thus, if the coefficient of friction is reduced using a larger R_{tip}, then adhesion problems can be avoided during the FSI characterization of these kinds of 2D materials.

Efforts will follow the inclusion of adhesion effects created by electrostatics forces during the friction between the tip/sample surface contacts in the FE simulation.

On the other hand, the quantification and explanation of the electrostatic forces generation by proximity of AFM tip and sample will be performed experimentally in a future work.

4. Conclusions

This work shows the adhesion effects of an FS arrangement for a three-layer GO sheet with an oxidation degree of 1.8. Strong adhesion for the case of the AFM cantilever tip was attributed to the mechanical-chemical effects of the rough surface produced by the hydroxy (32 %) and epoxy (43 %) groups present. In the study with Berkovich tip, the loss of oxygen groups was related to wrinkle flattening. The findings of this work contribute to dismissing the effects of adhesion, with the measurement technique having a more significant impact and associated with this, the size of the tip used to carry out the nanoindentation deformation. In the case of AFM, the deformation is more localized on an FS section of the GO sheet, while with the Berkovich tip, the section covered by the tip is larger.

This is an important condition when it is considered a larger R_{tip}, since offers some experimental advantages: (I) a large R_{tip} disperses the stresses along the bigger contact decreasing the COF and evading the formation of concentrated deformation, resulting in stable elastic deformations with lower adhesion effects, a regime where most of the FS indentation analysis takes place; and (II) a large R_{tip} increase the load for a similar displacement than those obtained by a small R_{tip}, which reduces the difficulties about experimental *FN* and *FT* resolution, as shows the comparison between our two experimental nanoindentation test. Therefore, our study with the current decreased adhesion effect can be applied to extend further investigations under these two conditions can be applied for the characterization of other 2D materials.

CRediT authorship contribution statement

E. Alejandra Huitrón Segovia: Investigation, Methodology, Data curation, Writing – original draft. **D. Torres-Torres:** Supervision, Data curation, Resources, Visualization, Formal analysis, Writing – review & editing. **A. García-García:** Conceptualization, Supervision, Project administration, Resources, Formal analysis, Writing – review & editing.

Declaration of competing interest

The authors declare that they have no known competing financial interests or personal relationships that could have appeared to influence the work reported in this paper.

Data availability

No data was used for the research described in the article.

References

[1] S.C. Ray, Application and uses of graphene oxide and reduced graphene oxide, in: Appl. Graphene Graphene-Oxide Based Nanomater, 2015, pp. 39–55, https://doi.org/10.1016/b978-0-323-37521-4.00002-9, no. December 2015.
[2] S. Deng, V. Berry, Wrinkled, rippled and crumpled graphene: an overview of formation mechanism, electronic properties, and applications, Mater. Today 19 (4) (2016) 197–212, https://doi.org/10.1016/j.mattod.2015.10.002.
[3] K. Sampathkumar, et al., Sculpturing graphene wrinkle patterns into compliant substrates, Carbon 146 (2019) 772–778, https://doi.org/10.1016/j.carbon.2019.02.041. N. Y.
[4] Q.Y. Lin, et al., Stretch-induced stiffness enhancement of graphene grown by chemical vapor deposition, ACS Nano 7 (2) (2013) 1171–1177, https://doi.org/10.1021/nn3053999.
[5] C. Lee, X. Wei, J.W. Kysar, J. Hone, Measurement of the elastic properties and intrinsic strength of monolayer graphene, Science (80-.) 321 (5887) (2008) 385–388, https://doi.org/10.1126/science.1157996.
[6] Z. Budrikis, S. Zapperi, Temperature-dependent adhesion of graphene suspended on a trench, Nano Lett. 16 (1) (2016) 387–391, https://doi.org/10.1021/acs.nanolett.5b03958.
[7] L. Zhou, Y. Wang, G. Cao, Boundary condition and pre-strain effects on the free standing indentation response of graphene monolayer, J. Phys. Condens. Matter 25 (47) (2013), https://doi.org/10.1088/0953-8984/25/47/475303.
[8] S. Park, D.A. Dikin, S.T. Nguyen, R.S. Ruoff, Graphene oxide sheets chemically cross-linked.pdf, J. Phys. Chem. C 113 (36) (2009) 15801–15804, https://doi.org/10.1021/jp907613s.
[9] X. Shen, X. Lin, N. Yousefi, J. Jia, J.K. Kim, Wrinkling in graphene sheets and graphene oxide papers, Carbon 66 (2014) 84–92, https://doi.org/10.1016/j.carbon.2013.08.046. N. Y.
[10] M.R. Begley, T.J. Mackin, Spherical indentation of freestanding circular thin films in the membrane regime, J. Mech. Phys. Solids 52 (9) (2004) 2005–2023, https://doi.org/10.1016/j.jmps.2004.03.002.
[11] G. Cao, H. Gao, Mechanical properties characterization of two-dimensional materials via nanoindentation experiments, Prog. Mater. Sci. 103 (February) (2019) 558–595, https://doi.org/10.1016/j.pmatsci.2019.03.002.

[12] A. Marti, G. Hähner, N.D. Spencer, Sensitivity of frictional forces to pH on a nanometer scale: a lateral force microscopy study, Langmuir 11 (12) (1995) 4632–4635, https://doi.org/10.1021/la00012a009.
[13] E.Alejandra Huitrón Segovia, D. Torres-Torres, J.Raúl Pérez Higareda, A. García-García, Indentation size effects in graphene oxide under suspended nanoindentation, Mech. Mater. 158 (August 2020) (2021), https://doi.org/10.1016/j.mechmat.2021.103875.
[14] C.S. Ruiz-Vargas, et al., Softened elastic response and unzipping in chemical vapor deposition graphene membranes, Nano Lett. 11 (6) (2011) 2259–2263, https://doi.org/10.1021/nl200429f.
[15] J. Wan, J.W. Jiang, H.S. Park, Negative Poisson's ratio in graphene oxide, Nanoscale 9 (11) (2017) 4007–4012, https://doi.org/10.1039/c6nr08657h.
[16] A. Allahbakhsh, F. Sharif, S. Mazinani, The influence of oxygen-containing functional groups on the surface behavior and roughness characteristics of graphene oxide, Nano 8 (4) (2013) 1–8, https://doi.org/10.1142/S1793292013500458.
[17] M.J. Woźniak, J. Ryszkowska, T. Szymborski, G. Chen, T. Tateishi, K. J. KurzydŁowski, Application of phase imaging and force modulation mode for description of dispersion of carbon nanotubes in polyol matrix, Mater. Sci. Pol. 26 (1) (2008) 245–253.
[18] S. Wang, Y. Zhang, N. Abidi, L. Cabrales, Wettability and surface free energy of graphene films, Langmuir 25 (18) (2009) 11078–11081, https://doi.org/10.1021/la901402f.
[19] K.T. Park, J. Choi, S.J. Sung, J. Park, T. Kim, C.R. Park, Surface energy modification of graphene oxide film by silanization co-functionalized with fluorine to maximize the moisture barrier property, Synth. Met. 277 (May) (2021), 116770, https://doi.org/10.1016/j.synthmet.2021.116770.
[20] A. Kozbial, et al., Study on the surface energy of graphene by contact angle measurements, Langmuir 30 (28) (2014) 8598–8606, https://doi.org/10.1021/la5018328.
[21] B. Gupta, N. Kumar, K. Panda, V. Kanan, S. Joshi, I. Visoly-Fisher, Role of oxygen functional groups in reduced graphene oxide for lubrication, Sci. Rep. 7 (2017) 1–14, https://doi.org/10.1038/srep45030.
[22] A. Lerf, H. He, M. Forster, J. Klinowski, Structure of graphite oxide revisited, J. Phys. Chem. B 102 (23) (1998) 4477–4482, https://doi.org/10.1021/jp9731821.
[23] H. Yang, J.S. Li, X. Zeng, Correlation between molecular structure and interfacial properties of edge or basal plane modified graphene oxide, ACS Appl. Nano Mater. 1 (6) (2018) 2763–2773, https://doi.org/10.1021/acsanm.8b00405.
[24] J. Dai, G. Wang, L. Ma, C. Wu, Study on the surface energies and dispersibility of graphene oxide and its derivatives, J. Mater. Sci. 50 (11) (2015) 3895–3907, https://doi.org/10.1007/s10853-015-8934-z.
[25] G. Yildiz, M. Bolton-Warberg, F. Awaja, Graphene and graphene oxide for bio-sensing: general properties and the effects of graphene ripples, Acta Biomater. 131 (2021) 62–79, https://doi.org/10.1016/j.actbio.2021.06.047.
[26] J. Han, S. Ryu, D.K. Kim, W. Woo, D. Sohn, Effect of interlayer sliding on the estimation of elastic modulus of multilayer graphene in nanoindentation simulation, Epl 114 (6) (2016), https://doi.org/10.1209/0295-5075/114/68001.
[27] J.R. Felts, et al., Direct mechanochemical cleavage of functional groups from graphene, Nat. Commun. 6 (2015), https://doi.org/10.1038/ncomms7467.
[28] K. Wang, J. Cheng, S. Yao, Y. Lu, L. Ji, D. Xu, Determination of electrostatic force and its characteristics based on phase difference by amplitude modulation atomic force microscopy, Nanoscale Res. Lett. 11 (1) (2016), https://doi.org/10.1186/s11671-016-1765-2.
[29] Jie Xu, Jinze Li, Wei Li, Calculating electrostatic interactions in atomic force microscopy with semiconductor samples, AIP Adv. 9 (10) (2019), 105308.